J|A|C|S ARTICLES

Published on Web 06/02/2010

Combined Multimodal Optical Imaging and Targeted Gene Silencing Using Stimuli-Transforming Nanotheragnostics

Min Suk Shim,[†] Chang Soo Kim,[†,‡] Yeh-Chan Ahn,[‡] Zhongping Chen,[†,‡,§] and Young Jik Kwon*[,†,§,||]

Department of Chemical Engineering and Materials Science, Beckman Laser Institute, and Departments of Biomedical Engineering and Pharmaceutical Sciences, University of California, Irvine, California 92697

Received January 21, 2010; E-mail: kwonyj@uci.edu

Abstract: Combined diagnosis and therapy for cancer has been of great interest in medicine. Small interference RNA (siRNA)-encapsulating polyplexes were covalently coated with small gold nanoparticles (Au NPs) via acid-cleavable linkages in order to explore the possibility of achieving combined stimuli-responsive multimodal optical imaging and stimuli-enhanced gene silencing. In a mildly acidic tumor environment, Au NPs are dissociated from the siRNA-carrying polyplexes, generating various optical signal changes such as diminished scattering intensity, increased variance of Doppler frequency, and blue-shifted UV absorbance (stimuli-responsive imaging). Simultaneously, Au NP dissociation exposes the siRNA-carrying polyplex with elevated surface charge and results in enhanced cellular uptake and transfection (stimuli-enhanced therapy). In this study, the feasibility of achieving combined diagnosis and therapy for cancer (theragnostics) is demonstrated by (1) microscopic and spectrophotometric confirmation of acid-transformation of the nanoparticles, (2) reduced scattering intensity and increased variance of Doppler frequency in an acidic pH upon the nanoparticle's transformation, and (3) simultaneous optical signal changes and gene silencing in vitro under a tumor pH-mimicking condition. This novel type of stimuli-responsive nanotheragnostics will provide a new paradigm for pinpointed, multimodal, and combined imaging and therapy for cancer.

Introduction

Imaging and therapy play crucial roles in prevention, early diagnosis, efficient treatment, and confirmation of complete cure. They also mutually and synergistically affect optimal prognosis for many diseases, especially cancer.[1,2] These two critical pillars were traditionally regarded as separately achievable (i.e., stepwise applied diagnosis and therapy), which was frequently found to be inconvenient, ineffective, and economically unfavorable. Recently, there has been great interest in developing nanomaterials that are capable of pinpointing abnormal lesions with molecular specificity, while converting the nanomaterials themselves to be therapeutic effectors in the pinpointed areas (i.e., nanotheragnostics).[3,4] Ideal nanotheragnostics, therefore, (1) differentiate biological events in cancer development/progress at a molecular level, (2) generate distinctive imaging signals in response to a biological trigger (e.g., pH, enzyme, hypoxia, and temperature), and (3) simultaneously convert themselves to activated therapeutic agents upon detecting a molecular event.

In this study, a single nanoparticle platform, which generates dramatic stimuli-responsive optical signal changes and is simultaneously activated for internalization and gene silencing, was developed for combined and synergistic optical imaging and gene therapy. Optical coherence tomography (OCT) that utilizes a low coherence light source is a noninvasive and high-speed imaging modality for obtaining micrometer-resolution images of tissue structure and velocity fluctuation (Brownian motion) of scattering particles.[5−9] However, obtaining clear-cut and pinpointed optical signals from different organizational and structural heterogeneity in a tissue has been a major challenge for OCT, which has been explored by employing absorption dyes and contrast agents as well as polarization sensitive OCT.[9] Among various OCT contrast agents for obtaining enhanced optical signals, gold nanoparticles (Au NPs) are promising OCT contrasting agents.[9] Au NPs offer high biocompatibility, easy functionalization, and useful optical properties such as surface plasmon resonance (SPR) effects that

[†] Department of Chemical Engineering and Materials Science, University of California, Irvine.
[‡] Beckman Laser Institute, University of California, Irvine.
[§] Department of Biomedical Engineering, University of California, Irvine.
[||] Department ofPharmaceutical Sciences, University of California, Irvine.

(1) Loo, C.; Lowery, A.; Halas, N.; West, J.; Drezek, R. *Nano Lett.* **2005**, *5*, 709–711.
(2) Huang, X.; El-Sayed, I. H.; Qian, W.; El-Sayed, M. A. *J. Am. Chem. Soc.* **2006**, *128*, 2115–2120.
(3) Hirsch, L. R.; Stafford, R. J.; Bankson, J. A.; Sershen, S. R.; Rivera, B.; Price, R. E.; Hazle, J. D.; Halas, N. J.; West, J. L. *Proc. Natl. Acad. Sci. U.S.A.* **2003**, *100*, 13549–13554.
(4) Lal, S.; Clare, S. E.; Halas, N. J. *Acc. Chem. Res.* **2008**, *41*, 1842–1851.
(5) Ding, Z. *Opt. Lett.* **2002**, *27*, 243–245.
(6) Drexler, W. *J. Biomed. Opt.* **2004**, *9*, 47–74.
(7) Ahn, Y.-C.; Jung, W.; Chen, Z. *Lab Chip* **2008**, *8*, 125–133.
(8) Wang, L.; Wang, Y.; Guo, S.; Zhang, J.; Bachman, M.; Li, G.; Chen, Z. *Opt. Commun.* **2004**, *242*, 345–350.
(9) Kim, C. S.; Wilder-Smith, P.; Ahn, Y.-C.; Liaw, L.-H. L.; Chen, Z.; Kwon, Y. J. *J. Biomed. Opt.* **2009**, *14*, 034008.

10.1021/ja100580y © **2010 American Chemical Society**

can be controlled by modulating Au NPs' sizes and shapes.[9−14] In addition to elevated contrasts by differentially distributing Au NPs in a tissue, it is highly desirable to achieve optical signal changes triggered by molecular events in a diseased lesion (stimuli-responsive imaging).

It is hypothesized that covalently clustered Au NPs via cancer stimuli-cleavable linkages on the small interfering RNA (siRNA)-encapsulating polyplexes will accomplish stimuli-responsive optical identification of cancer lesions and stimuli-enhanced gene silencing. In normal tissues, the Au NPs remain clustered, generating strong scattering intensity by high SPR effects due to interparticle coupling effects. However, cancer-specific stimuli break the linkages, causing the clustered Au NP to dissipate into smaller individual particles and generate dramatic drops in scattering intensity by lost interparticle coupling effects.[15−18] In addition, smaller particles in a tumor tissue generate a significantly higher variance of Doppler frequency due to their fast Brownian motion.[19−22] Theoretically, Au NP aggregates have a red-shifted maximum UV absorbance peak, while individual particles have a blue-shifted one.[23] Therefore, the maximum UV absorbance will be blue-shifted upon Au NPs' disassembly in a tumor tissue. Finally, disassembled Au NPs will diffuse out of tissue more rapidly than clustered particles, which will also generate different time-dependent optical signal changes in cancer and normal tissues.

Linear polyethylenimine grafted with acid-degradable amino ketal branches (ketalized linear PEI, KL-PEI) was employed as a platform for Au NPs to be anchored via stimuli-responsive linkages. KL-PEI has been demonstrated to be an efficient and biocompatible siRNA delivery carrier.[24] It was shown that KL-PEI's acid-hydrolysis rate in the intracellular endosomes (e.g., pH 5.0) was estimated to be approximately 3 times faster than in the mildly acidic extracellular space of tumor tissues[24] where the pH was reported to be as low as 6.0.[25−27] This means that ketal branches on the surface of the KL-PEI/nucleic acid polyplexes are likely to be hydrolyzed in a tumor tissue. The nucleic acid-complexing core would be fully disassembled after reaching the intracellular endosome where the pH is significantly lower than that of extracellular areas.

To achieve molecular optical imaging and simultaneous gene silencing in mildly acidic tumor tissue, the stimuli-transforming nanoparticles were designed as following: (1) Au NPs are conjugated on the surface of the siRNA/KL-PEI polyplex to carry both an optical contrast agent (Au NPs) and therapeutic nucleic acids (siRNA), (2) Au NPs are conjugated with siRNA/KL-PEI polyplexes via acid-cleavable amines on the surface of the polyplexes for Au NPs' disassembly at a mildly acidic pH, and (3) the outer Au NP layers on the polyplexes are PEGylated to prevent aggregation of the nanoparticles and to interfere with cellular internalization of siRNA/KL-PEI polyplexes until extracellular acidic pH disassembles Au NPs (siRNA/KL-PEI-Au NP-PEG). Figure 1 shows the hypothetic nanoparticle for stimuli-triggered, combined OCT imaging and cancer gene therapy. In normal tissue, Au NPs are covalently immobilized on the polyplex surface, generating high scattering, low variance of Doppler frequency, red-shifted UV absorbance, and slow transport. The PEG and Au NP-layers prevent cells from internalizing the nanoparticles (Figure 1A). In tumor tissue, however, mildly acidic extracellular pH degrades ketal linkages mainly on the surface of the nanoparticles (Scheme 1), and liberated individual Au NPs generate dramatically decreased scattering intensity, increased variance of Doppler frequency, and blue-shifted UV absorbance (Figure 1B). In addition, the individual Au NPs' significantly smaller size enables the body to clear them efficiently. Cells in tumor tissue actively take up the siRNA-encapsulating core without the PEGylated Au NP shell due to its fully exposed cationic surface and reduced size (Figure 1C). Then the internalized polyplex core releases siRNA from the destabilized endosome into the cytoplasm, upon rapid acid-hydrolysis, followed by silenced target gene expression (steps 1−3 in Figure 1C).

Herein, Au NP-shelled siRNA-carrying nanoparticles were synthesized, and their acid-transformation and accompanying property changes, such as acid-responsive disassembly of Au NPs, size reduction, surface charge increase, and blue-shifted UV absorbance were confirmed by using various microscopic and spectroscopic tools. In addition, the optical signal changes simultaneously generated by such phenomena were imaged and quantified by OCT. Finally, enhanced gene silencing in association with distinctive optical signal changes in a mildly acidic tumor pH was demonstrated in vitro.

Experimental Section

Materials. Linear polyethylenimine (2.5 kDa) was purchased from Polyscience, Inc. (Warrington, PA). Hydrogen tetrachloroaurate (III) trihydrate ($HAuCl_4 \cdot 3H_2O$) and sodium citrate (Na_3-citrate) were purchased from Sigma Aldrich (Milwaukee, WI). *N*-Succinimidyl 3-(2-pyridyldithio)-propionate (SPDP) and PEG monomethyl ether (0.6 kDa) were purchased from Pierce (Rockford, IL). 2-Aminoethanol, pyridinium *p*-toluenesulfonate, ethyl trifluoroacetate, 2-methoxypropene, 4-dimethylaminopyridine (DMAP), and molecular sieves were supplied by Acros (Morris Plains, NJ). Acryloyl chloride was supplied by Alfa Aesar (Ward Hill, MA). Dithiothreitol (DTT) was supplied by Fisher Scientific (Pittsburgh, PA). Spectra/Por cellulose ester dialysis membranes (MWCO = 500 Da) were purchased from Spectrum Laboratories (Rancho Dominguez, CA). A carbon-coated copper TEM grid was purchased from Electron Microscopy Sciences (Hatfield, PA). Silencer eGFP

(10) Sokolov, K.; Follen, M.; Aaron, J.; Pavlova, I.; Malpica, A.; Lotan, R.; Richards-Kortum, R. *Cancer Res.* **2003**, *63*, 1999–2004.
(11) Gobin, A. M.; Lee, M. H.; Halas, N. J.; James, W. D.; Drezek, R. A.; West, J. L. *Nano Lett.* **2007**, *7*, 1929–1934.
(12) Oldenburg, A.; Zweifel, D. A.; Xu, C.; Wei, A.; Boppart, S. A. *Proc. SPIE Int. Soc. Opt. Eng.* **2005**, *5703*, 50–60.
(13) Loo, C.; Lin, A.; Hirsch, L.; Lee, M. H.; Barton, J.; Halas, N.; West, J.; Drezek, R. *Technol. Cancer Res. Treat.* **2004**, *3*, 33–40.
(14) Lee, T. M.; Oldenburg, A. L.; Sitafalwalla, S.; Marks, D. L.; Luo, W.; Toublan, F. J.-J.; Suslick, K. S.; Boppart, S. A. *Opt. Lett.* **2003**, *28*, 1546–1548.
(15) Sonnichsen, C.; Reinhard, B. M.; Liphardt, J.; Alivisatos, A. P. *Nat. Biotechnol.* **2005**, *23*, 741–745.
(16) Su, K. H.; Wei, Q. H.; Zhang, X.; Mock, J. J.; Smith, D. R.; Schultz, S. *Nano Lett.* **2003**, *3*, 1087–1090.
(17) Wang, H.; Levin, C. S.; Halas, N. J. *J. Am. Chem. Soc.* **2005**, *127*, 14992–14993.
(18) Khlebtsov, B.; Zharov, V.; Melnikov, A.; Tuchin, A.; Khlebtsov, N. *Nanotechnology* **2006**, *17*, 5167–5179.
(19) Ren, H.; Brecke, K. M.; Ding, Z.; Zhao, Y.; Nelson, J. S.; Chen, Z. *Opt. Lett.* **2002**, *27*, 409–411.
(20) Wilder-Smith, P.; Hammer-Wilson, M. J.; Zhang, J.; Wang, Q.; Osann, K.; Chen, Z.; Wigdor, H.; Schwartz, J.; Epstein, J. *Clin. Cancer Res.* **2007**, *13*, 2449–2454.
(21) Varghese, B.; Rajan, V.; Van Leeuwen, T. G.; Steenbergen, W. *Rev. Sci. Instrum.* **2007**, *78*, 126103.
(22) Jang, S. P.; Choi, S. U. S. *Appl. Phys. Lett.* **2004**, *84*, 4316–4318.
(23) Storhoff, J. J.; Music, R. C.; Mirkin, C. A. *J. Cluster Sci.* **1997**, *8*, 179–216.
(24) Shim, M. S.; Kwon, Y. J. *Bioconjugate Chem.* **2009**, *20*, 488–499.
(25) Engin, K.; Leeper, D. B.; Cater, J. R.; Thistlethwaite, A. J.; Tupchong, L.; McFarlane, J. D. *Int. J. Hyperthermia* **1995**, *11*, 211–216.
(26) Stubbs, M.; McSheehy, P. M. J.; Griffiths, J. R. *Adv. Enzyme. Regul.* **1999**, *39*, 13–30.
(27) Fischer, B.; Muller, B.; Fischer, K.-G.; Baur, N.; Kreutz, W. *Clin. Immunol.* **2000**, *96*, 252–263.

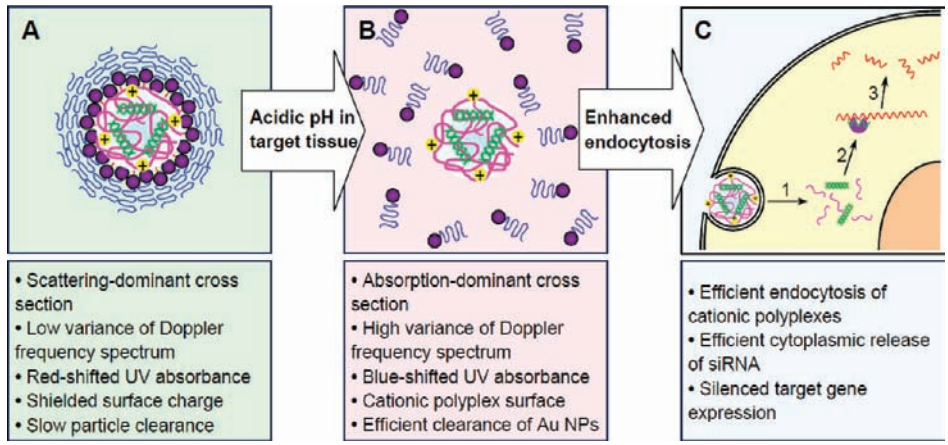

Figure 1. Schematic diagram of hypothetic acid-triggered transformation of siRNA/KL-PEI-Au NP-PEG nanoparticles. Au NPs (purple) are immobilized on the surface of a siRNA-encapsulating core (pink, KL-PEI; green, siRNA) via acid-cleavable ketal linkages (red). To prevent aggregation of the siRNA/KL-PEI-Au NP nanoparticles, the Au NP's surface is further conjugated with PEG (blue). (A) Without stimuli, Au NPs are clustered together, behaving like large Au NPs and hiding the siRNA/KL-PEI core. (B) In a mildly acidic extracellular environment in tumor tissue, ketal linkages are hydrolyzed, liberating individual Au NPs and exposing the cationic polymer/siRNA core. (C) The exposed cationic surface and reduced size of the polymer/siRNA cores enable cells to actively internalize them. Upon rapid hydrolysis of acid-degradable branches in the endosome, the polyplex releases siRNA into the cytoplasm (step 1 in C), released siRNA is processed and binds the cellular machinery (i.e., RNA-induced silencing complex, RISC) (step 2 in C), and target mRNA is cleaved so that target gene expression is silenced (step 3 in C).

Scheme 1. (A) Synthesis of Ketalized Linear PEI (KL-PEI) and (B) siRNA Release and Au NP Dissociation under a Mildly Acidic Condition[a]

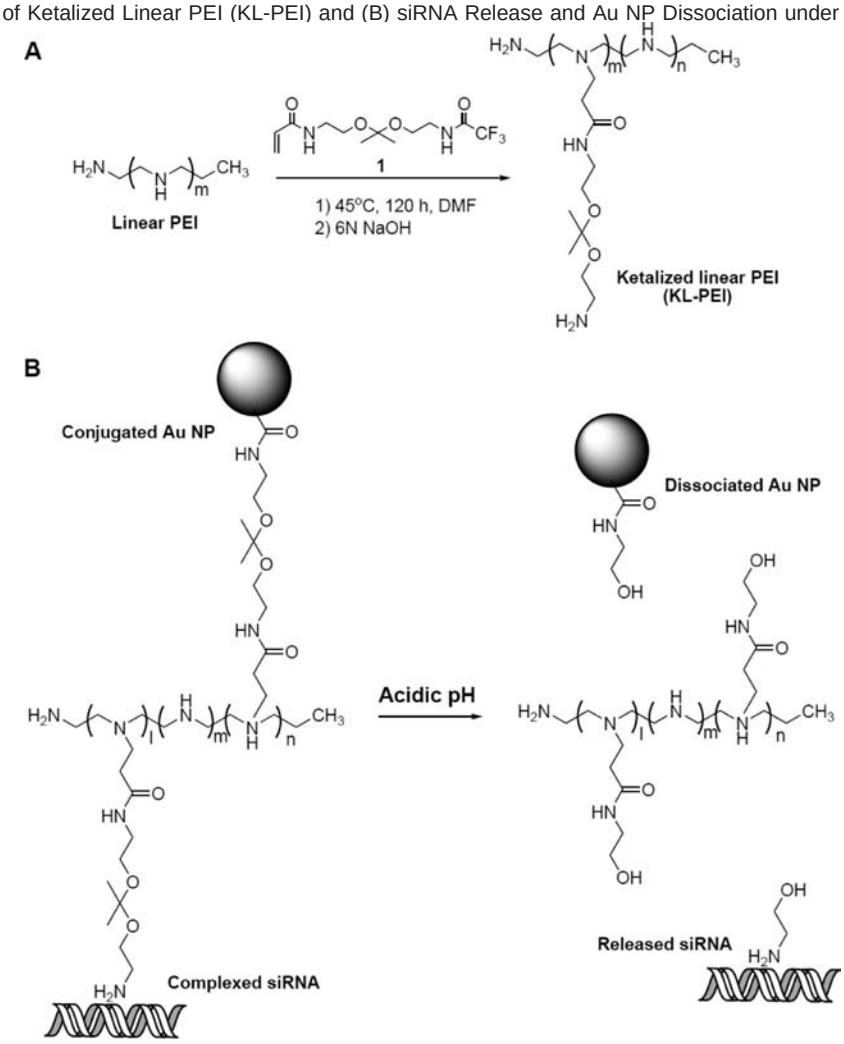

[a] It should be noted that Au NPs conjugated on the surface are dissociated in a mildly acidic tumor tissue (e.g., pH 6.0), due to their full exposure, before siRNA in the core polyplex is released in the more acidic endosome (pH 5.0).

siRNA (sense strand 5′-CAAGCUGACCCUGAAGUUCdTdT-3′ and antisense strand 5′-GAACUUCAGGGUCAGCUUGdCdC-3′), negative control siRNA (sense strand 5′-AGUACUGCUUAC-GAUACGGdTdT-3′ and antisense strand 5′-CCGUAUCGUAAG-CAGUACUdTdT-3′), and FAM-labeled negative control siRNA (sense strand 5′-FAM-AGUACUGCUUACGAUACGGdTdT-3′ and antisense strand 5′-CCGUAUCGUAAGCAGUACUdTdT-3′) were purchased from Ambion (Austin, TX). NIH 3T3 cells (ATCC, Rockville, MD) were cultured in Dulbecco's modified Eagle's medium (DMEM) (MediaTech, Herndon, VA) with 10% fetal bovine serum (FBS) (Hyclone, Logan, UT), unless otherwise noted. GFP ELISA and BCA protein analysis kits were purchased from Cell Biolabs (San Diego, CA) and Pierce (Rockford, IL), respectively.

Synthesis of Ketalized Linear Polyethylenimine (KL-PEI). The synthesis of acid-degradable ketalized linear polyethylenimine (KL-PEI), which was reported previously,[24] was further optimized to obtain the maximally efficient form of the polymer (Scheme 1A). Briefly, linear low molecular weight PEI (L-PEI, MW 2.5 kDa) (0.13 g, 3.0 mmol of secondary amine groups, 1 equiv) dissolved in 2 mL of methanol was dried under high vacuum for 30 min. The resulting liquid polymer was dissolved in 10 mL of dimethylformamide (DMF), followed by mixing with 1.87 g of compound **1** (Scheme 1A) (6.0 mmol, 2 equiv) and 0.15 g of triethylamine (1.5 mmol, 0.5 equiv). The resulting mixture was stirred for 120 h at 45 °C, and the polymer was precipitated into anhydrous diethyl ether at room temperature and dried under vacuum. After trifluoroacetate groups at the end of ketal branches were deprotected by 6 N NaOH, the polymer was purified by dialysis (MW cutoff = 500) against DI water at 4 °C. Ketalization ratios relative to available secondary amines were determined to be approximately 34% by integral ratios of the peak at 1.41 ppm to the peak at 2.7−3.0 ppm using ^{1}H NMR spectroscopy as described previously.[24]

Preparation of SPDP-Activated Au NPs. Gold nanoparticles (Au NPs, 15 nm in diameter) were synthesized by Frens method[28] with slight modifications. One hundred milliliters of $HAuCl_4 \cdot 3H_2O$ (0.01% w/w) solution was heated at its boiling point, followed by mixing with 4 mL of Na_3-citrate (1% w/w) solution with vigorous stirring. The resulting solution was refluxed for an additional 15 min and allowed to cool down to room temperature with continuous stirring. All glassware was cleansed in aqua regia (HCl:HNO_3 in 3:1 ratio by volume) and thoroughly rinsed with distilled water. All chemicals were dissolved in ultrapure deionized (DI) water (18.2 MΩ). The size of the final Au NPs was determined using a Phillips CM 20 transmission electron microscope (TEM) (Philips Electronic Instruments, Mahwah, NJ) and ZEN3600 Zetasizer dynamic light scattering (DLS) particle analyzer (Malvern Instruments, Worcestershire, U.K.). The concentration of the resulting Au NPs was calculated to be 1.56×10^{11} particles/mL using the UV/vis spectroscopic method as shown previously.[29] To activate Au NPs for conjugation with siRNA/KL PEI polyplexes, 10 mL of Au NPs redispersed in 0.02 M sodium bicarbonate solution (pH = 8.73) were gradually added to 20 mM SPDP solution (2 μL) in DMSO using a syringe pump at the 7 μL/s flow rate while vigorously stirring on ice. The mixture was stirred overnight at room temperature, and unreacted SPDP was removed by centrifugation twice at 7500*g* for 30 min. The conjugation was repeated again to ensure saturated SPDP-activation of Au NPs. The SPDP-activated Au NPs were kept at 4 °C without exposure to light, and the resulting SPDP-conjugated Au NPs were resuspended in DI water immediately before use.

The amount of SPDP on the Au NPs was quantified by the release of pyridine-2-thione group in the presence of dithiothreitol (DTT). Briefly, 1.7 mL of SPDP-conjugated Au NP solution in 0.02 M sodium bicarbonate was washed twice with DI water by centrifugation at 7500*g* for 30 min. After 85 μL of DTT solution (15 mg/mL in DI water) was added to 0.85 mL of SPDP-Au NP solution, the mixture was incubated for 15 min at room temperature, and the absorbance at 343 nm was measured using a Varian Cary 50 UV/vis Spectrophotometer (Varian Inc., Palo Alto, CA). The background absorbance by 85 μL of DI water and 0.85 mL of SPDP-Au NP solution was also measured. The number of SPDP in 0.85 mL of SPDP-Au NP solution was calculated to be 4.85 nmol (4.73×10^{-20} mol SPDP per Au NP) using the extinction coefficient of pyridine-2-thione at 343 nm (i.e., 8.08×10^3 M^{-1} cm^{-1}).

Preparation of siRNA/KL-PEI-Au NP-PEG Nanoparticles. Forty micrograms of siRNA and 1.13 mg of KL-PEI (3.06 μmol of primary amine groups in KL-PEI) were mixed in 800 μL of DI water to obtain an amine to phosphate (N/P) ratio of 100, followed by incubation for 30 min at room temperature. SPDP-Au NPs in DI water (800 μL, 4.56 nmol of Au NP-conjugated SPDP) were concentrated into 160 μL of solution by centrifugation at 7500*g* for 30 min. The siRNA/KL-PEI polyplex-containing solution (800 μL) was slowly added to the concentrated SPDP-Au NP solution in the presence of 0.5 μg of 4-dimethylaminopyridine (DMAP) (4.10 nmol) at 4 °C, and the mixture was stirred overnight at 4 °C. Finally, amine-functionalized PEG monomethyl ether (mPEG-NH_2, 0.6 kDa) (1.33 μmol in 8 μL of DI water) was added, and the resulting reaction mixture was further stirred for 8 h at 4 °C. Unreacted Au NPs and mPEG-NH_2 were removed by centrifugation at 2000*g* for 30 min.

Characterization of siRNA/KL-PEI-Au NP-PEG Nanoparticles. Mean particle diameter (Z-average) and zeta potential of siRNA/KL-PEI-Au NP-PEG nanoparticles resuspended in 960 μL of DI water were measured at 25 °C by using a ZEN3600 Zetasizer. The mean values of each sample from at least 10 measurements were obtained. The size and morphological changes of siRNA/KL-PEI-Au NP-PEG nanoparticles upon acid-hydrolysis were further analyzed by TEM. For TEM analysis, a 4 μL aliquot of the sample solution was dropped on a carbon-coated copper TEM grid and air-dried overnight. To hydrolyze the nanoparticles, 480 μL of 100 mM acetate buffer (adjusted by NaOH to pH 5.0) was mixed with 240 μL of the siRNA/KL-PEI-Au NP-PEG nanoparticle solution, resulting in the final pH of 5.0 for the mixed buffer. After 2 h of incubation at 37 °C, the resulting solution was analyzed for size, surface charge, UV absorbance, and morphology, as described earlier. For DLS analysis, a 72 μL aliquot of the hydrolyzed polyplex-containing solution was diluted with additional 800 μL of DI water.

Prehydrolysis of siRNA/KL-PEI-Au NP-PEG Nanoparticles Prior to Incubation with Cells. To simulate activation of siRNA/KL-PEI-Au NP-PEG nanoparticles for intracellular internalization upon Au NP dissociation, the solution (240 μL in DI water) containing 10 μg (750 pmol) of siRNA (eGFP silencer siRNA for RNA interference and FAM-labeled siRNA for cellular internalization analysis) in the nanoparticles was mixed with 480 μL of pH 5.0 acetate buffer, resulting in the unchanged pH of 5.0. During incubation at 37 °C, an aliquot of siRNA/KL-PEI-Au NP-PEG (72 μL, 1 μg of siRNA) nanoparticle-containing solution was taken at different time points (e.g., 5, 10, 20, 30, and 60 min) for evaluation of cellular internalization and RNA interference.

Internalization of siRNA/KL-PEI-Au NP-PEG Nanoparticles and RNA Interference. For internalization analysis, NIH 3T3 cells were inoculated in 24-well culture plates at a density of 4×10^4 cells/well in 0.5 mL of DMEM containing 10% FBS. After 24 h of incubation, the medium was replaced with 351 μL of FBS-free DMEM (or 303 μL of FBS-free DMEM before adding the prehydrolyzed nanoparticle). Then, a 24 μL aliquot of FAM-labeled-siRNA/KL-PEI-Au NP-PEG nanoparticle solution containing 1 μg (75 pmol) of labeled siRNA or 72 μL of prehydrolyzed FAM-labeled-siRNA/KL-PEI-Au NP-PEG nanoparticle solution was added to the cells (final siRNA concentration of 200 nM). After 1 h of incubation, the cells were washed with PBS three times.

(28) Frens, G. *Nature* **1973**, *241*, 20–22.
(29) Haiss, W.; Thanh, N. T.; Aveyard, J.; Fernig, D. G. *Anal. Chem.* **2007**, *79*, 4215–4221.

The amounts of internalized FAM-labeled siRNA were quantified by the mean fluorescence intensity of the cells using a Guava EasyCyte Plus cytometer (Guava Technologies, Hayward, CA).

eGFP-expressing NIH 3T3 cells were obtained by retroviral transduction and subsequent G418 selection.[30] To evaluate RNA interference, the eGFP-expressing NIH 3T3 cells were seeded in a 24-well plate at a density of 1.6×10^4 cells/well. After 24 h, the culture medium in each well was replaced with 351 μL of FBS-free DMEM (or 303 μL of FBS-free DMEM before adding the prehydrolyzed nanoparticle). Then, a 24 μL aliquot of siRNA/KL-PEI-Au NP-PEG nanoparticle solution containing 1 μg (75 pmol) of siRNA or a 72 μL of prehydrolyzed siRNA/KL-PEI-Au NP-PEG nanoparticle solution was added to the cells in order to obtain a final siRNA concentration of 200 nM. Free Au NPs were also incubated with the cells to confirm their effects on eGFP expression. After 4 h of incubation, the medium in the well was replaced with 0.5 mL of fresh DMEM containing 10% FBS, followed by an additional 68 h-incubation. Then, the cells were lysed, and eGFP amount in the cell lysate was quantified by GFP enzyme-linked immunosorbent assay (ELISA), according to manufacturer's protocols, and further normalized by the total protein amount quantified by a BCA protein assay kit. The sequence-specific gene silencing by siRNA was also confirmed by comparing gene expression levels of the cells incubated with control siRNA with scrambled sequences. The eGFP expression in the cells incubated with the same amount of free Au NPs used for siRNA/KL-PEI-Au NP-PEG nanoparticles was also quantified.

Acquisition and Analysis of Scattering Intensity and Doppler Variance Images of siRNA/KL-PEI-Au NP-PEG Nanoparticles-Containing Droplets. The siRNA/KL-PEI-Au NP-PEG nanoparticle solution (960 μL) was concentrated to 10 μL of solution by centrifugation at 2000*g* for 30 min. The resulting solution (3 μL) was mixed with 6 μL of DI water as a control, and 7 μL of the solution was mixed with 14 μL of pH 5.0 acetate buffer to hydrolyze the nanoparticles. After 2 h of incubation at 37 °C, a 3 μL aliquot of each sample was dropped on the polyethylene substrate, and the scattering intensity and Doppler variance images were obtained using spectral domain (SD)-OCT. The detailed setup for SD-OCT and calculation of Doppler variance are described in Supporting Information (Figure S1). Three-dimensional OCT images were constructed using 2-D images (512 × 512 pixels) with 512 frames using the Amira program (Visage Imaging, Inc., San Diego, CA). Doppler variance images of the nanoparticle-containing solutions with and without acid-hydrolysis were quantified by Image J software which is a public domain Java image processing program developed by the NIH. After an area of 100 × 100 pixels was chosen under the vertex of the droplet, the relative number (%) of pixels for each color from the selected area was quantified and represented as a histogram.

Simultaneous Optical Imaging and Gene Silencing in Vitro. eGFP-expressing NIH 3T3 cells were cultured in a Falcon 8-well culture slide (BD Biosciences, Franklin Lakes, NJ) at an initial seeding density of 1.6×10^4 cells/well. After 24 h, the culture medium was replaced with 90 μL of serum-free, CO_2-independent medium (Invitrogen, Carlsbad, CA) supplemented with 30 mM 3-(*N*-morpholino)propanesulfonic acid (MOPS) and 30 mM 2-(*N*-morpholino)ethanesulfonic acid (MES) (pH 6.0). Then, a 24 μL aliquot of siRNA/KL-PEI-Au NP-PEG nanoparticle solution containing 1 μg (75 pmol) of siRNA was added to the cells in order to obtain a final siRNA concentration of 200 nM. For comparison, the cells were also incubated with the nanoparticles in serum-free CO_2-independent medium without MOPS and MES (pH 7.3). While the cells were incubated with nanoparticles at room temperature for different periods of time (e.g., 10, 20, and 30 min), scattering intensity and Doppler variance images were obtained. All the images (512 × 512 pixels) were obtained with the SD-OCT shown in Supporting Information (Figure S1). Scattering intensity SD-OCT and Doppler variance images were obtained with 4 and 20 times line average, respectively. The scattering intensity and variance of Doppler frequency in the nanoparticle-containing media were quantified by Image J software. Intensity histograms of randomly picked areas (500 × 300 pixels) in the scattering intensity images were averaged (a repeated total three frames of SD-OCT) as weighted means. To quantify averaged variance of Doppler frequency, variance of Doppler frequency histograms of randomly picked areas (200 × 200 pixels) were used.

After optical imaging at 10, 20, and 30 min, the acidic MOPS/MES medium was neutralized by adding 260 μL of DMEM containing 8 μmol of NaOH (the final of pH 7.3). The same amount of NaOH-free DMEM was added to the cells incubated with neutral MOPS- and MES-free medium. After the cells were further incubated for another 4 h-transfection at 37 °C, the medium in the well was replaced with 0.5 mL of fresh DMEM containing 10% FBS. After incubation for an additional 68 h, gene silencing efficiency defined by reduced green fluorescence intensity of a cell was observed under an Olympus IX71fluorescence microscope (Olympus America, Melville, NY).

Statistical Analysis. Triplicate data were analyzed using one-way ANalysis Of VAriance (ANOVA) on the significance level of $p < 0.01$ and presented as mean ± standard deviation.

Results and Discussion

Synthesis, Characterization, and Acid-Transformation of siRNA/KL-PEI-Au NP-PEG Nanoparticles. To conjugate Au NPs with siRNA/KL-PEI polyplexes, 15 nm Au NPs were functionalized with SPDP which was anchored on the Au NP surface via pyridyldithio groups while providing free amine-reactive *N*-succinimidyl (NHS) groups for conjugation with the siRNA/KL-PEI polyplex. Since the NHS group had higher reactivity toward primary amines over secondary and tertiary amines, Au NPs were conjugated mainly with primary amine-bearing ketal branches, resulting in siRNA/KL-PEI polyplexes with an outer Au NP shell. Then, the remaining unreacted NHS groups on the surface of the Au NP shell were conjugated with amine-functionalized PEG (0.6 kDa), which is known to prevent Au NP aggregation, decrease clearance by reticuloendothelial system (RES), and interfere with cellular uptake by steric hindrance.[31] Conjugation of SPDP-activated Au NPs on the siRNA/KL-PEI polyplexes was confirmed by FT-IR (Figure S2, Supporting Information). Inductively coupled plasma optical emission spectrometry (ICP-OES) showed 83% conjugation efficiency of SPDP-activated Au NPs on the siRNA/KL-PEI polyplexes (Table S1, Supporting Information). The size and surface charge of the resulting siRNA/KL-PEI-Au NP-PEG nanoparticles were measured to be 194.4 nm (DLS) and +17.2 (±1.27) mV (zeta-potential analysis), respectively (Figure 2A). To confirm dissociation of Au NP-PEG from the polyplexes upon acid-hydrolysis with decreased size and increased zeta-potential, the nanoparticles were incubated in pH 5.0 acetate buffer for 2 h at 37 °C. The size of the acid-hydrolyzed nanoparticles split to 114.6 nm (hydrolyzed polymer/siRNA aggregates, 94.5% intensity) and 19.12 nm (Au NP-PEG, 5.5% intensity, solid arrow) by losing PEGylated Au NP shells (Figure 2A). Incubation of the nanoparticles in acidic buffers that were at the same pH but different electrolyte concentrations (i.e., 10 and 100 mM acetate buffers adjusted to pH 5.0 by NaOH) did not result in differences in size (data not shown), confirming that the acidic pH (not different electrolyte concentrations)

(30) Kwon, Y. J.; Yu, H.; Peng, C.-A. *Biotechnol. Bioeng.* **2001**, *72*, 331–338.

(31) Otsuka, H.; Nagasaki, Y.; Kataoka, K. *Adv. Drug Delivery Rev.* **2003**, *55*, 403–419.

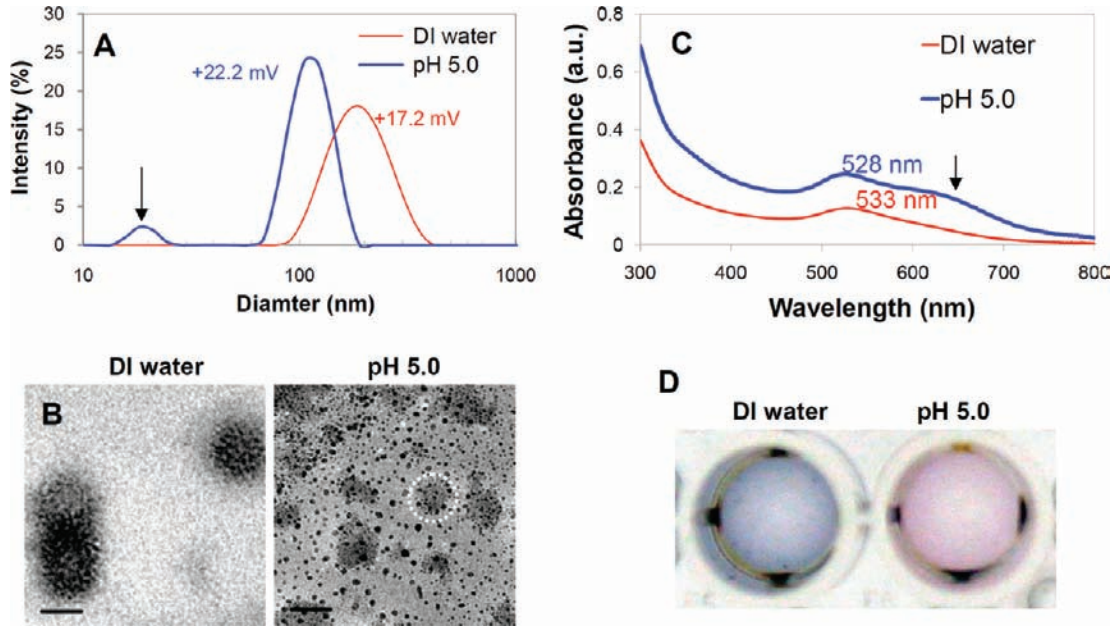

Figure 2. Acid-responsive changes of siRNA/KL-PEI-Au NP-PEG nanoparticles' physical properties. (A) Size of the nanoparticles measured by DLS before (red) and after (blue) acid-hydrolysis for 2 h at pH 5.0. Arrow indicates disassembled Au NPs at an acidic pH. Numbers are the zeta-potentials of the nanoparticles before hydrolysis (red) and the acid-hydrolyzed nanoparticles including dissociated Au NPs and hydrolyzed siRNA/KL-PEI polyplexes (blue). (B) TEM images of siRNA/KL-PEI-Au NP-PEG nanoparticles before (left) and after (right) acid-hydrolysis. The dotted area indicates a siRNA/KL-PEI polyplex after Au NPs and PEG are dissociated. Scale bar =100 nm. (C) UV absorbance by the nanoparticles before (red) and after (blue) acid-hydrolysis for 2 h. The arrow indicates the absorbance by residual aggregates. (D) Colorimetric changes of the solutions (200 μL in a 96-well plate) containing siRNA/KL-PEI-Au NP-PEG nanoparticles before (left) and after (right) hydrolysis at pH 5.0 for 10 min.

reduced the size of Au NP-siRNA/KL-PEI-PEG nanoparticles. It should be emphasized that the relative volumes of dissociated Au NPs and siRNA/polymer aggregates were 93.4 and 6.6%, respectively, indicating that most of the Au NPs were dissociated from polyplexes. Transmission electron micrographs also proved that most Au NPs were completely liberated from siRNA/KL-PEI polyplexes upon acid-hydrolysis (Figure 2B). The zeta-potential of siRNA/KL-PEI polyplexes, which was originally +25.95 (±1.90) mV, decreased to +17.2 mV with Au NP- and PEG-conjugations; however, incubation at pH 5.0 for 2 h restored the cationic surface charge to +22.2 (±1.20) mV by exposing the cationic siRNA/KL-PEI core (Figure 2A), which was expected to facilitate cellular uptake via attractive electrostatic interaction with negatively charged proteoglycans (e.g., heparan sulfate) as well as the phospholipid bilayer cellular membrane. Zeta-potential changes in various pH and electrolyte concentrations showed that the cationic conversion of Au NP-siRNA/KL-PEI-PEG nanoparticles was mainly attributed to pH changes (Figure S3, Supporting Information). To differentiate increased zeta-potential by protonation at pH 5.0, unketalized branched PEI (B-PEI, 25 kDa) was used to synthesize nonhydrolyzable Au NP-siRNA/B-PEI-PEG nanoparticles because KL-PEI resembles branched PEI due to its primary, secondary, and tertiary amines (Scheme 1). Incubation of the nonhydrolyzable nanoparticles in the same pH 5.0 acetate buffer resulted in increased zeta-potential of 2.4 (±0.71) mV. This indicates that the dissociation of Au NPs and protonation at pH 5.0 may equally contribute to cationic conversion of Au NP-siRNA/KL-PEI-PEG nanoparticles. B-PEI would have more primary amines than acid-hydrolyzed KL-PEI whose primary amine-bearing ketal branches are converted to neutral hydroxyl-bearing termini. Since primary amines have higher protonation capability than secondary and tertiary amines, the zeta-potential change of B-PEI at an acidic pH 5.0 may be overestimated than that of KL-PEI due to protonation at the same pH. This implies that the zeta-potential increase of Au NP-siRNA/KL-PEI-PEG nanoparticles at pH 5.0 was significantly more affected by the Au NP and PEG disassembly than protonation at an acidic pH.

The nanoparticles shelled with Au NPs showed the maximum UV absorbance wavelength (λ_m) at 533 nm, while hydrolysis resulted in λ_m at 528 nm, which is close to λ_m of pure 15 nm Au NPs (i.e., 520 nm).[32] The residual aggregates (not detectable by DLS), consisting of free Au NPs, siRNA/KL-PEI polyplexes, and/or hydrolyzed KL-PEI, resulted in slightly increased UV absorbance between 600 and 700 nm wavelength (arrow in Figure 2C). Disassembly of Au NPs from the nanoparticles upon acid-hydrolysis turned the color of the nanoparticles in DI water (blue) into a typical color of colloidal Au NPs (pink) (Figure 2D). The results shown in Figure 2 clearly present distinctive physical property changes upon dissociation of PEG-Au NPs from the surface of siRNA/KL-PEI polyplex cores.

Acid-Responsive Changes of siRNA/KL-PEI-Au NP-PEG Nanoparticles' Optical Properties. The possibility of utilizing the changes of siRNA/KL-PEI-Au NP-PEG nanoparticles' various physical properties under a mildly acidic condition (Figure 2) for detecting pathological signals in cancer using OCT was investigated (Figure 3). When small Au NPs (15 nm) were locally immobilized on the surface of siRNA/KL-PEI polyplex at a high density, higher optical scattering was obtained due to dramatically increased SPR effects (Figure 3A). Upon dissociation, however, small individual Au NPs were in an absorption-dominant cross section with negligible SPR effects, significantly reducing scattering intensity (Figure 3B). Few remaining strong signals from hydrolyzed nanoparticles could be explained by the presence of residual aggregates identified in Figure 2C. The Doppler variance images demonstrated that Brownian motion of the Au NPs that were dissociated from the siRNA/KL-PEI-

(32) Krpetić, Ž.; Nativo, P.; Porta, F.; Brust, M. *Bioconjugate Chem.* **2009**, *20*, 619–624.

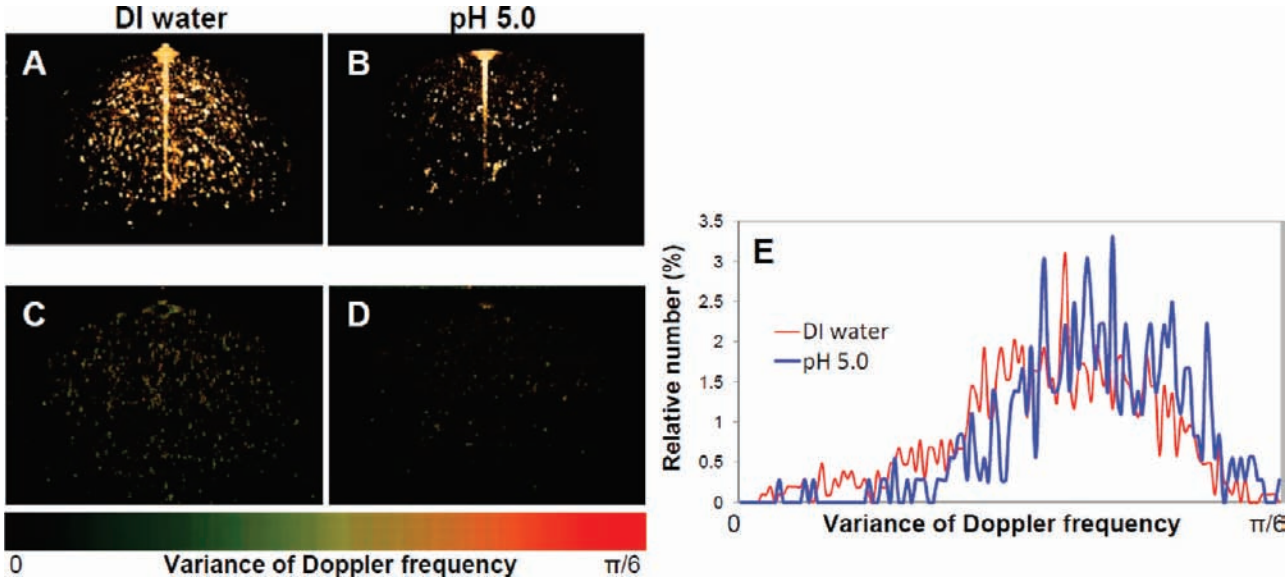

Figure 3. Optical coherence property changes of siRNA/KL-PEI-Au NP-PEG nanoparticles upon acid-hydrolysis. (A and B) Three-dimensional SD-OCT images of the droplet (3 μL) containing the nanoparticles before (A) and after (B) acid-hydrolysis. (C and D) Doppler variance images of the droplet containing the nanoparticles before (C) and after (D) acid-hydrolysis, represented by color codes (green, slow moving nanoparticles; red, fast moving nanoparticles). (E) Quantified distributions of the variance of Doppler frequency from C and D.

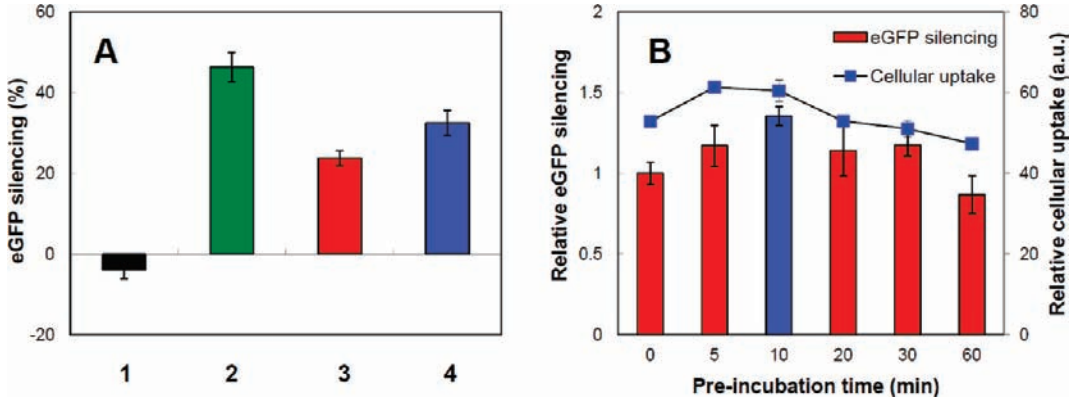

Figure 4. Stimuli-responsive activation of siRNA/KL-PEI-Au NP-PEG nanoparticles for gene silencing. (A) eGFP gene silencing efficiency of (1) free Au NPs, (2) siRNA/KL-PEI, (3) siRNA/KL-PEI-Au NP-PEG without prior incubation at pH 5.0, (4) siRNA/KL-PEI-Au NP-PEG incubated at pH 5.0 for 10 min. (B) Effects of preincubation of siRNA/KL-PEI-Au NP-PEG nanoparticles at pH 5.0 for different periods of time on cellular internalization and gene silencing. For cellular uptake analysis, NIH 3T3 cells were incubated with FAM-labeled siRNA-encapsulating siRNA/KL-PEI-Au NP-PEG nanoparticles for 1 h. Specific gene silencing was confirmed by comparing with that of scrambled siRNA-encapsulating nanoparticles which resulted in barely measurable gene silencing (data not shown).

Au NP-PEG nanoparticles in response to acidic stimuli was increased, which was represented by increased red color pixels in Figure 3D in comparison to Figure 3C. The increased variance of Doppler frequency was also quantitatively analyzed as shown in Figure 3E. The increase in Brownian movement was lower than what was expected (Figure 3E). According to the Stoke-Einstein equation, Au NPs are supposed to move more than 10 times faster than unhydrolyzed nanoparticles. This may be attributed to the increased viscosity of the hydrolyzed polymer-containing solution and changes in Au NP/hydrolyzed polymer interactions (e.g., increased encountering frequency between Au NPs). In addition, it is also possible that the currently available OCT technology has a limited capability of detecting all dissociated small individual Au NPs, as shown by diminished stimuli-responsive scattering intensity in Figure 3B. The results shown in Figure 3 indicate that cancer lesions can be more accurately identified by combining both scattering intensity and Doppler variance images with each other rather than relying on a single type of optical signal. Although the results shown in Figures 2 and 3 were obtained after 2 h-incubation at pH 5.0 in order to ensure complete hydrolysis, it was confirmed that 10 min of hydrolysis at the same pH was sufficient to generate almost equivalent physical property changes, hence, optical signal changes.

Enhanced Gene Silencing by Acid-Activated siRNA/KL-PEI-Au NP-PEG Nanoparticles. The hypothesis of achieving facilitated gene silencing associated with various optical signal changes was assessed. eGFP-expressing NIH 3T3 cells were incubated with siRNA/KL-PEI, siRNA/KL-PEI-Au NP-PEG nanoparticles before exposure to an acidic condition (Au NP-conjugated gene carriers before generating various optical property changes), and siRNA/KL-PEI-Au NP-PEG nanoparticles incubated at pH 5.0 for various periods of time (gene carriers with dissociated Au NPs). As shown in Figure 4A, conjugation of Au NPs and further PEGylation substantially reduced gene silencing efficiency by siRNA/KL-PEI polyplexes (from 46% to 24%) at a siRNA concentration of 200 nM. This can be explained by interfered cellular internalization by the

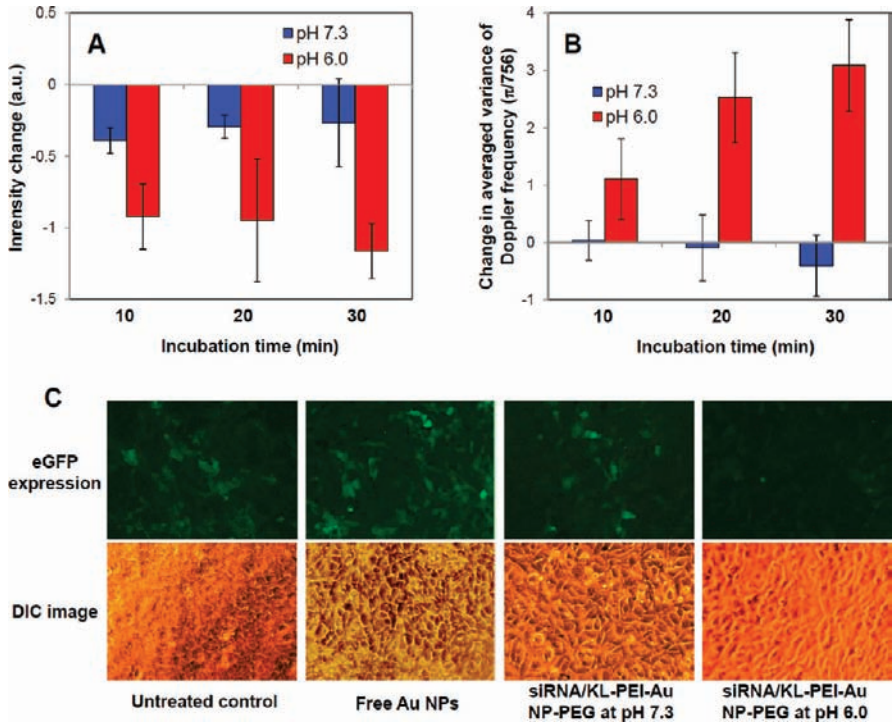

Figure 5. Stimuli-transformation of siRNA/KL-PEI-Au NP-PEG nanoparticles in vitro under a tumor-mimicking condition, generating (A) reduced light scattering intensity, (B) increased variance of Doppler frequency, and (C) enhanced gene silencing. eGFP-expressing NIH 3T3 cells were incubated with the nanoparticles at pH 7.3 or 6.0 for 10 min before being incubated at pH 7.3 for another 4 h for transfection in serum-free media. Gene silencing efficiency was observed after another 68 h-incubation in serum-containing media. Indistinctive gene silencing was observed when scrambled control siRNA was used, compared with that of untreated cells (data not shown).

outer PEG layer, low cationic surface charge, and increased size of polyplexes. On the other hand, conjugation of Au NPs and PEGylation improved the biocompatibility of siRNA/KL-PEI-Au NP-PEG nanoparticles by slightly lowering cytotoxicity (Figure S4, Supporting Information). Gene silencing quantified by reduced fluorescence of the cells, which were incubated under the same conditions, showed slightly less statistically significant results, possibly due to Au NPs' fluorescence interference (Figure S5, Supporting Information). Gene silencing efficiency is expected to increase with concentration, which necessitates the use of more cationic polymers. The cells incubated with siRNA/KL-PEI-Au NP-PEG nanoparticles at 100, 200, and 400 nM siRNA demonstrated concentration-proportional gene silencing but with decreasing viability (Figure S6, Supporting Information). Therefore, a siRNA concentration of 200 nM was used in this study in order to achieve optimized gene silencing and cell viability.

The hypothesis of achieving enhanced gene silencing via exposure of a size-reduced and cationic siRNA/KL-PEI polyplex core in the presence of stimuli was proven as shown in Figure 4B. Incubation of siRNA/KL-PEI-Au NP-PEG nanoparticles at pH 5.0 for 10 min before being incubated with the cells enhanced gene silencing by approximately 37% (Particle 4 in Figure 4A). Enhanced gene silencing efficiency of siRNA/KL-PEI-Au NP-PEG nanoparticles was closely correlated with cellular uptake of the nanoparticles preincubated at pH 5.0 for different periods of time (e.g., ~15% increased internalization after 10 min of preincubation, Figure 4B). The fact that it takes only ~10 min for siRNA/KL-PEI-Au NP-PEG nanoparticles to transform themselves into activated gene therapeutics (Figure 4B) implies that fast stimuli-responsive diagnosis and gene delivery can be achieved.

Simultaneous Multimodal Optical Signal Changes and Enhanced Gene Silencing in Vitro by siRNA/KL-PEI-Au NP-PEG Nanoparticles. The feasibility of achieving simultaneous multimodal optical imaging and enhanced gene silencing using stimuli-transforming siRNA/KL-PEI-Au NP-PEG nanoparticles was demonstrated in vitro (Figure 5). Physical and optical property changes of the siRNA/KL-PEI-Au NP-PEG nanoparticles (Figures 2 and 3) and enhanced gene silencing (Figure 4) were investigated at an endosomal pH 5.0. However, normal extracellular pH in a tumor is in the range of 6.0−7.2.[25−27] Therefore, the results shown in Figures 2−4 may not represent the acid-responsive optical signal changes and cationic activation of the nanoparticles in a slightly acidic tumor tissue, followed by rapid siRNA release from the more acidic endosome into the cytoplasm of a cell. It is also believed that the siRNA-encapsulating core could be partially hydrolyzed during the Au NP-PEG dissociation at pH 5.0 even for the 10 min of preincubation.

To demonstrate simultaneous optical imaging and transfection under a more realistic condition, eGFP-expressing cells were incubated with the siRNA/KL-PEI-Au NP-PEG nanoparticles at a tumor pH of 6.0 as well as physiological pH of 7.3. As shown in Figure 5A,B, 10 min-incubation at pH 6.0 resulted in reduced scattering intensity ($p = 0.02$) and substantially increased variance of Doppler frequency ($p = 0.009$). On the contrary, incubation at pH 7.3 even for 30 min resulted in minimal changes. While scattering intensity reached its maximum decrease after a 10 min-incubation at pH 6.0 medium and remained unchanged, variance of Doppler frequency increased with incubation time. This indicates that substantially increased Brownian motion requires a complete dissociation of individual Au NPs, but a partial dissociation of Au NPs from siRNA/KL-

PEI polyplexes is sufficient to diminish light scattering. Slightly decreased variance of Doppler frequency after 30 min-incubation of the siRNA/KL-PEI-Au NP-PEG nanoparticles at pH 7.3 may indicate partial aggregation.

The cells incubated with siRNA/KL-PEI-Au NP-PEG nanoparticles for 10 min at pH 7.3 and 6.0, followed by 4 h-transfection and additional incubation for 68 h at pH 7.3, were observed under a fluorescence microscope (Figure 5C). It is clear that the highest gene silencing was achieved when the cells were incubated with siRNA/KL-PEI-Au NP-PEG nanoparticles at a tumor pH of 6.0 for 10 min, while incubation of the cells with the nanoparticles at a physiological pH 7.3 resulted in moderate but significantly lower gene silencing ($p = 0.007$) than at pH 6.0. As shown in Figure 4B that a preincubation at pH 5.0 for 10 min maximally enhanced gene silencing efficiency of siRNA/KL-PEI-Au NP-PEG nanoparticles, the maximum gene silencing was obtained when the cells were incubated with the nanopartitcles at pH 6.0 for 10 min (Supporting Information, Figure S7). In this study, the cells were transfected by the siRNA/KL-PEI-Au NP-PEG nanoparticles under a serum-free condition. It was confirmed that the gene silencing by the siRNA/KL-PEI-Au NP-PEG nanoparticles was not affected in the 10% serum-containing media (data not shown), as previously reported using siRNA/KL-PEI polyplexes.[24] However, both scattering intensity and variance of Doppler frequency were reduced in the presence of serum without acid-responsiveness, indicating Au NP aggregation (and precipitation) which may be minimized by coating the surface of Au NPs with bovine serum albumin (BSA)[33,34] or polymers (e.g., polyvinyl alcohol, PVA).[35,36]

The results shown in Figure 5 propose the feasibility of obtaining multimodal optical imaging and enhanced transfection shortly after (i.e., 10 min) stimuli-transforming siRNA/KL-PEI-Au NP-PEG nanoparticles are accumulated (delivered) in a tumor tissue. The siRNA/KL-PEI polyplex core partially hydrolyzes during the Au NP-PEG dissociation at pH 6.0, although its hydrolysis in the endosomal pH of 5.0 is much faster. This implies that significantly improved stimuli-enhanced gene silencing could be achieved by tuning the nanoparticles to be differentially responsive to extracellular and intracellular stimuli (e.g., siRNA/KL-PEI conjugated with Au NPs via matrix metalloproteinases (MMPs)-cleavable linkages).[37,38]

Conclusions

A novel nanotheragnostic agent that transforms its optophysical properties in the presence of a cancer-specific stimulus was developed for combined optical imaging and gene therapy by conjugating small Au NPs on the surface of siRNA-carrying polyplexes via acid-degradable linkages. The hypothesis of achieving various optical signal changes (blue-shifted UV absorbance, diminished scattering intensity by lost SPR effects, and increased variance of Doppler frequency) with simultaneously enhanced cellular internalization and subsequent gene silencing was demonstrated using the stimuli-transforming nanoparticles. These novel nanotheragnostic materials could detect a pathological event and simultaneously trigger themselves to act on identified targets when they are further tuned and optimized for demonstration in vivo. The use of this novel theragnostics concept could be expanded by incorporating other types of therapeutic agents (e.g., chemoagents) and imaging contrast agents (e.g., magnetic iron oxide nanoparticles) for different modes of combined imaging and therapy applications as well as using various polymers responding to other types of disease-specific and external stimuli, such as enzymes, hypoxia, redox potential gradients, temperature, and light.

Acknowledgment. The authors thank Dr. Jill E. Millstone (UC Berkeley) and Mr. Yang Han (UC Irvine) for assistance with gold quantification by ICP-OES and FT-IR analysis, respectively. This work was financially supported by the NIH (3R21DE19298-02S1, EB-00293, CA-91717, RR-01192), AFOSR (FA9550-04-1-0101), the Beckman Laser Institute Endowment, the UC Cancer Center Support Grant (5P30CA062203-13), and Council on Research Computing and Libraries Multi-Investigator Award (MI 23-2009-2010, UC Irvine).

Supporting Information Available: OCT setup, analysis of Doppler variance images, FT-IR spectroscopy, quantification of Au NPs by ICP-OES, electrolyte concentration effects on nanoparticles' zeta-potential changes, cytotoxicity of the nanoparticles, quantification of eGFP silencing by flow cytometry, and in vitro gene silencing efficiency at various siRNA concentrations and different pH conditions. This material is available free of charge via the Internet at http://pubs.acs.org.

JA100580Y

(33) Gao, D.; Tian, Y.; Liang, F.; Ding, L.; Bi, S.; Chen, Y.; Zhang, H.; Yu, A. *Colloids Surf., B* **2006**, *47*, 71–77.
(34) Housni, A.; Ahmed, M.; Liu, S.; Narain, R. *J. Phys. Chem. C* **2008**, *112*, 12282–12290.
(35) Tcherniak, A.; Ha, J. W.; Dominguez-Medina, S.; Slaughter, L. S.; Link, S. *Nano Lett.* **2010**, *10*, 1398–1404.
(36) Basu, S.; Pande, S.; Jana, S.; Bolisetty, S.; Pal, T. *Langmuir* **2008**, *20*, 5562–5568.
(37) Overall, C. M.; Kleifeld, O. *Nat. Rev. Cancer* **2006**, *6*, 227–239.
(38) Hatakeyama, H.; Akita, H.; Kogure, K.; Oishi, M.; Nagasaki, Y.; Kihira, Y.; Ueno, M.; Kobayashi, H.; Kikuchi, H.; Harashima, H. *Gene Ther.* **2007**, *14*, 68–77.